Journal of the Association of Arab Universities for Basic and Applied Sciences (2017) **23**, 29–36

University of Bahrain

Journal of the Association of Arab Universities for Basic and Applied Sciences

www.elsevier.com/locate/jaaubas
www.sciencedirect.com

ORIGINAL ARTICLE

2-Amino-4-(2,4-dihydroxyphenyl) quinoline-3-carbonitrile as sustainable corrosion inhibitor for SAE 1006 steel in 1 M HCl: Electrochemical and surface investigation

Chandrabhan Verma, M.A. Quraishi *

Department of Chemistry, Indian Institute of Technology, Banaras Hindu University, Varanasi 221005, India

Received 5 October 2015; revised 4 February 2016; accepted 13 March 2016
Available online 16 April 2016

KEYWORDS

SAE 1006 steel;
Acid solution;
Corrosion;
Mixed type;
SEM–EDX/AFM;
Quantum chemical calculations

Abstract The corrosion inhibition efficiency of 2-amino-4-(2,4-dihydroxyphenyl) quinoline-3-carbonitrile (ADQC) on SAE 1006 steel has been investigated using electrochemical (EIS and Polarization), surface (SEM, EDX and AFM) and quantum chemical calculation methods. Results showed that inhibition efficiency increases with increasing ADQC concentration and maximum value of 96.12% was obtained at 25 mg/L concentration. EIS results showed the ADQC inhibits SAE 1006 steel corrosion becoming the adsorbate at metal/electrolyte interfaces. Polarization study showed that ADQC acts as cathodic type inhibitor. SEM, EDX and AFM finding supported the adsorption of ADQC on the mild steel surface. The quantum chemical calculations provide good insight about the adsorption and inhibition mechanism of ADQC. The experimental and quantum chemical calculation results were in good agreement.

1. Introduction

SAE 1006 steel and its alloys have been successfully used in many applications such as chemical processing, petroleum production and refining, construction and metal processing equipment because of their high mechanical strength and low cost (Abd El-Lateef, 2015; Verma et al., 2015a). However, they easily undergoe corrosion by chemical and electrochemical reactions with the environments which causes severe safety and economic problems. Among the several available methods, the use of synthetic corrosion inhibitors is the most common, effective and economic method of metallic corrosion protection (Yadav et al., 2013). The adsorption of these inhibitors on metal surface is influenced by molecular volume, planarity of the molecule, availability of lone pair of electrons present on the heteroatoms (S, N, O), polarity and dipole moment, presence of unsaturation or aromatic ring, and energy of frontier molecular orbitals (Verma et al., 2015b). Further, literature survey reveals that compounds containing nitrile (–CN) group act as efficient metallic corrosion inhibitors (Verma et al., 2015c; El Azzouzi et al., 2015). However, the increasing ecological awareness and strict environmental

* Corresponding author. Tel.: +91 9307025126; fax: +91 542 2368428.
E-mail addresses: maquraishi.apc@itbhu.ac.in, maquraishi@rediffmail.com (M.A. Quraishi).
Peer review under responsibility of University of Bahrain.

http://dx.doi.org/10.1016/j.jaubas.2016.03.002
1815-3852

regulations throughout the world needed development of the green corrosion inhibitors with high inhibition efficiency at low environmental risk. In this context, multicomponent reactions that combine three or more reacting molecules have immersed as a green and powerful technique, as several biologically active complex molecules can be synthesized in one step with high yield (Beattie et al., 2011). Further, utilization of the environmental friendly solvents and chemicals is of particular importance as they contribute many of the green chemistry principles. Due to its non-flammable, non-hazardous, non-toxic, uniquely redox-stable, inexpensive and free availability, water as reaction medium has drawn significant attention in this direction. Moreover, in asymmetric organocatalysis, consumption of the L-proline particularly in water and ionic liquids is the most sustainable method as it is directly isolated from the natural sources without use of any hazardous chemicals and solvents such as DMSO, DMF and other chlorinated solvents (Sheldon, 2005; Nezhad et al., 2012).

In view of this, in the present study we have reported the corrosion inhibition property of 2-amino-4-(2,4-dihydroxyphenyl) quinoline-3-carbonitrile (ADQC) on SAE 1006 steel in 1 M HCl using electrochemical impedance spectroscopy, Tafel polarization, scanning electron microscopy (SEM), energy dispersive X-ray spectroscopy (EDX), atomic force microscopy (AFM) and quantum chemical calculation methods. The novelty of the present work is that 2-amino-4-(2,4-dihydroxyphenyl) quinoline-3-carbonitrile used in the present study shows very high inhibition efficiency and utilized for the first time. The high inhibition efficiency of the studied compound is attributed due to presence of two aromatic and one hetero-aromatic rings and several polar functional groups (such as –CN, –OH, $–NH_2$) that act as adsorption centers.

2. Experimental procedure

2.1. Materials and chemicals

All electrochemical and surface studies were performed on SAE 1006 steel specimens containing 0.076 wt.% C, 0.192 wt.% Mn, 0.012 wt.% P, 0.026 wt.% Si, 0.050 wt.% Cr, 0.023 wt.% Al, and balance with Fe. The specimens and electrolytic solution of 1 M HCl were prepared as described earlier (Verma et al., 2016).

2.2. Synthesis of inhibitor

The investigated inhibitor was synthesized using previously described method (Nezhad et al., 2012) as shown in Fig. 1. The progress and completion of the reaction were monitored by TLC method. The purity of the synthesized compound was also determined by single spot on the TLC plate. The synthesized compound was characterized by IR (KBr, 1/cm) and 1H NMR spectral data. The characterization data of the synthesized compound are as follows: Yield: 82%; IR (KBr, 1/cm) 3684, 3426, 3142, 2262, 2858, 1654, 1560, 1436, 830, 624, ^{1}H NMR (300 MHz, CDCl3, δ, ppm): 7.12–7.23, 7.68–7.98, 8.30, 8.42, 8.69.

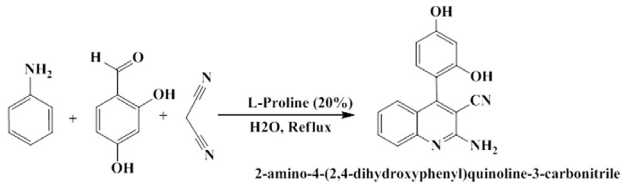

Figure 1 Synthetic scheme for investigated ADQC.

2.3. Electrochemical experiments

The conventional three electrode glass cell assembly consisting of a pure platinum mesh counter electrode, a saturated calomel reference electrode and SAE 1006 steel specimen working electrode was used for all electrochemical measurements. The Tafel and EIS measurements were carried out using a Gamry Potentiostat/Galvanostat (Model G-300) with EIS software Gamry Instruments Inc., USA. Echem. Analyst 5.0 software package was applied to fit and analyze all the electrochemical data. In polarization measurements, the cathodic and the anodic Tafel slopes were plotted by varying the electrode potential inevitably from −0.25 to +0.25 V vs. corrosion potential (E_{corr}) at a constant sweep rate of 1.0 mV s^{-1}. The corrosion current density (i_{corr}) was obtained by extrapolating the linear segments of the cathodic and anodic Tafel slopes from which percentage of inhibition efficiency (η%) was calculated using the following relation (Verma et al., 2013):

$$\eta\% = \frac{i^0_{corr} - i^i_{corr}}{i^0_{corr}} \times 100 \quad (1)$$

where, i^0_{corr} and i^i_{corr} are the corrosion current densities in the absence and presence of the ADQC at different concentrations, respectively.

The electrochemical impedance studies were carried out under potentiodynamic condition in a frequency range of 100 kHz–0.01 Hz. The amplitude of the AC sinusoid wave was 10 mV. All electrochemical studies were performed in naturally aerated solution of 1 M HCl in the absence and presence of different concentration of ADQC after 30 min immersion time. The charge transfer resistances (R_{ct}) were calculated from the diameter of the Nyquist plots by using which inhibition efficiency (η%) at different studied concentrations was calculated using the following relationship (Verma et al., 2013):

$$\eta\% = \frac{R^i_{ct} - R^0_{ct}}{R^i_{ct}} \times 100 \quad (2)$$

where, R^0_{ct} and R^i_{ct} are the charge transfer resistances in the absence and presence of ADQC at different concentrations, respectively.

2.4. Morphological investigation

For surface study, the SAE 1006 steel specimens having exposed dimension 1 cm^2 were immersed in 1 M HCl for 3 h in the absence and presence of optimum concentration of ADQC. After elapsed time the specimens were taken out washed and cleaned with distilled water, dried and finally analyzed. A SEM model Ziess Evo 50 XVP was employed to carry out SEM analysis. The elements present on the metal surface were studied by energy dispersive X-ray spectroscopy (EDX) coupled with SEM. The atomic force microscopic (AFM) measurements were performed using a NT-MDT multimode AFM, Russia, controlled by Solver scanning probe microscope

controller containing NOVA programme. The scanning areas were 5 μm × 5 μm during AFM measurements in the absence and presence of the ADQC.

2.5. Quantum chemical calculations

Quantum chemical calculations were carried out for ADQC using the density functional theory (DFT) method involving the Becke three-parameter hybrid functional together with the Lee–Yang–Paar correlation functional (B3LYP) (Becke, 1993). The 6-31 + G (d, p) basis set was chosen for all the calculations. The calculations were carried out with the aid of Gaussian 09 software for Windows (Revision D.01) (Frisch et al., 2009). The gas phase optimized geometries of the compound were confirmed to correspond to its true energy minima by the absence of imaginary frequency in the computed vibrational frequencies. All quantum chemical parameters were derived based on the electronic parameters of the most stable conformers of the molecule. The frontier molecular orbital (FMO) energies, that is, the highest occupied molecular orbital energy (E_{HOMO}) and the lowest unoccupied molecular energy (E_{LUMO}) were calculated. Other parameters such as the energy gap (ΔE), global hardness (σ), and global softness (ρ), were computed respectively according to the equations (Martinez, 2003; Olasunkanmi et al., 2015):

$$\Delta E = E_{LUMO} - E_{HOMO} \tag{3}$$

$$\sigma = \frac{1}{2}(E_{LUMO} - E_{HOMO}) \tag{4}$$

where, η was approximated to the chemical hardness of the inhibitor molecule. Selected dihedral angles that might have some correlations with the experimental inhibition efficiency of the compounds were also reported.

3. Results and discussion

3.1. Electrochemical measurements

3.1.1. Open circuit potential vs time curves

Potential developed on working electrode relative to the potential of the reference electrode without applying any external current is regarded as open circuit potential (E_{OCP}). The stabilization of the E_{OCP} prior to electrochemical experiment is necessary. After 30 min immersion time in the absence and presence of the AQDC at different concentration, the E_{OCP} curves were measured for two minutes. The E_{OCP} curves of working electrode with time (s) in 1 M HCl are shown in Fig. 2. The strength lines of the E_{OCP} vs time curves in the absence and presence of inhibitor suggested that steady state potential has been established in both the cases. From Fig.2 it can be seen that in the presence of AQDC, the E_{OCP} shifted toward more negative direction. This shift of the E_{OCP} toward nobler direction in the presence of inhibitor is attributed due to dissolution of surface oxide layer (Yadav and Quraishi, 2012). Further, the shift of the E_{OCP} toward negative direction also attributed due to adsorption of the AQDC on metallic surface (Sudheer and Quraishi, 2014). This finding suggests that AQDC inhibits metallic corrosion by becoming adsorbate at the metallic surface.

3.1.2. Potentiodynamic polarization study

The potentiodynamic polarization nature of SAE 1006 steel specimens in the absence and presence of different studied concentrations of the ADQC is shown in Fig. 3. From the Figure it was observed that presence of ADQC causes significant change in the anodic and cathodic half reactions. The values of electrochemical kinetic parameters such as corrosion potential (E_{corr}), corrosion current density (i_{corr}) and anodic and cathodic Tafel slopes (β_a, β_c), and percentage of inhibition efficiency (η%) were determined by the Tafel extrapolation method and are given in Table 1. From the results it can be observed that inhibition efficiency increases with increasing ADQC concentrations and maximum value of 95.77% was obtained at 25 mg/L concentration. Inspection of the results reveals that in the presence of ADQC, the values of the i_{corr} decrease significantly and therefore η% increases due to blocking of the active sites present on the metallic surface (Feng

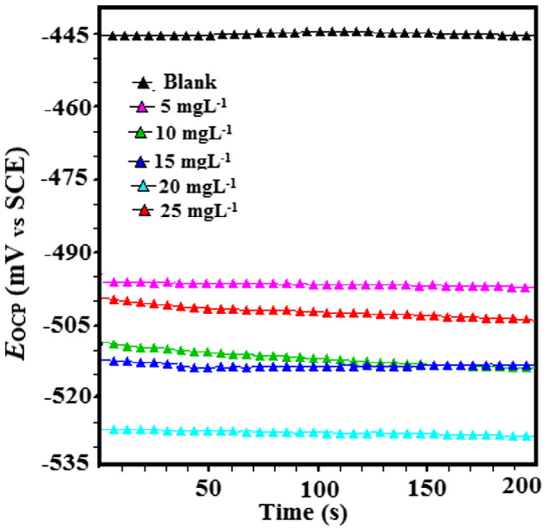

Figure 2 Chrono-potentiometric (zero current) curves for mild steel in 1 M HCl in the absence and presence of optimum concentrations of different ADQC.

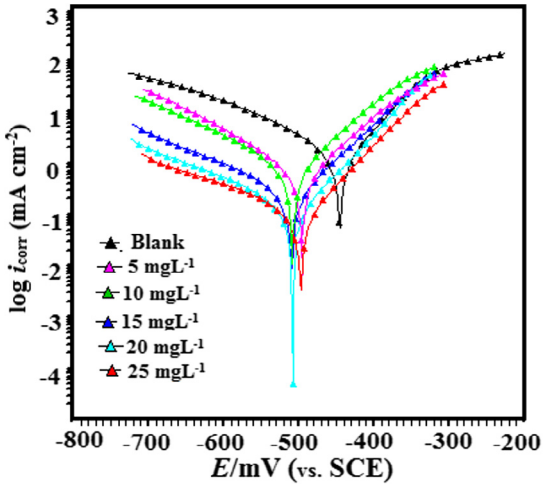

Figure 3 Potentiodynamic polarization curves for mild steel in the absence and presence of different concentrations of ADQC.

Table 1 Tafel polarization parameters for mild steel in 1 M HCl solution in the absence and at different concentration of ADQC.

Inhibitor	Conc (mg/L)	E_{corr} (V/SCE)	i_{corr} (μA/cm)	β_a (mV/dec)	β_c (mV/dec)	θ	η%
Blank	–	−445	1150	70.5	114.6	–	–
ADQC	5	−496	612.7	76.30	96.0	0.4672	46.72
	10	−508	128.3	80.20	136.1	0.8883	88.83
	15	−511	98.7	59.90	144.6	0.9141	91.41
	20	−527	73.9	83.50	135.2	0.9357	93.57
	25	−498	48.6	75.60	137.2	0.9577	95.77

et al., 2011). Further, from the results depicted in Table 1 and Fig. 3 it is observed that the values of β_a and β_c both were affected in the presence of ADQC at different concentrations; however, the change in the values of β_c was more prominent as compared to the change in the values of β_a, suggesting the investigated inhibitor acts as cathodic type inhibitor (Li et al., 2009).

3.1.3. Electrochemical impedance spectroscopy (EIS) study

The Nyquist plots in the absence and presence of different studied concentrations of the ADQC are shown in Fig. 4a.

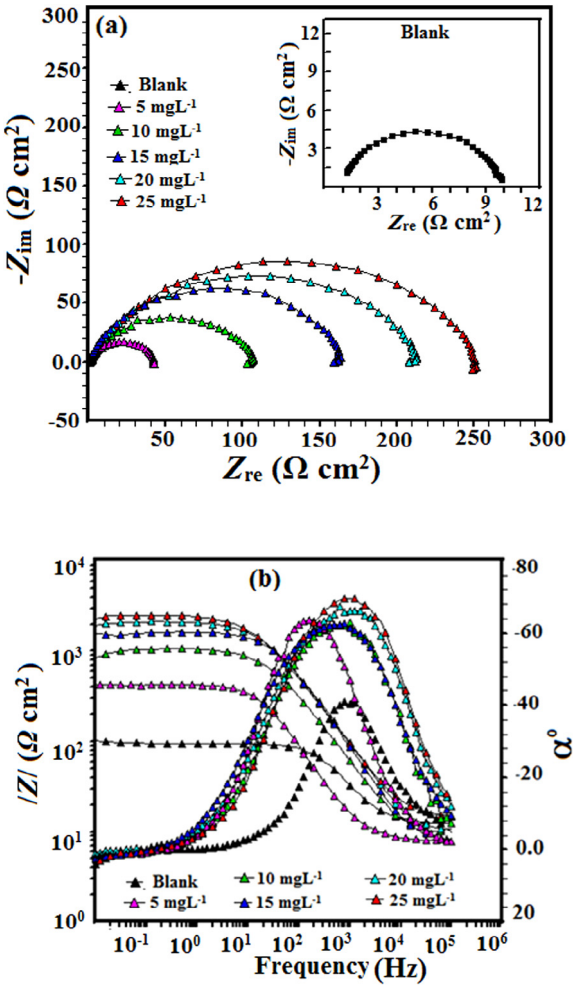

Figure 4 (a) Nyquist plots for mild steel in the absence and presence of different concentrations of ADQC, (b) Bode plots for mild steel in the absence and presence of different concentrations of ADQC.

Nyquist plots give one semicircle in the absence and presence of different concentrations of ADQC suggesting that inhibition of metallic corrosion taking place in the present study is due to retardation of electron charge transfer process which is confirmed by single maxima in the Bode plots. Deviation from the perfect semicircle is generally attributed to the frequency dispersion as well as to the inhomogeneities of the surface and mass transport resistant (Seikh and Sherif, 2015). Examination of the Fig. 4a shows that in the presence of ADQC the diameter of the Nyquist plots increases with increasing concentration. The increased diameter of the Nyquist plots in the presence of ADQC suggested that values of charged transfer resistance (R_{ct}) increase due to formation of protective film. The impedance parameters were derived using equivalent circuit described elsewhere (Verma et al., 2014) and are given in Table 2. The equivalent circuit consists of solution resistance (R_s), charge transfer resistance (R_{ct}) and a constant phase element (CPE). The values of R_{ct} in the absence and presence of different concentrations of ADQC were obtained by fitting EIS data in this equivalent circuit. From the calculated values of R_{ct}, the value of double layer capacitance (C_{dl}) in the absence and presence of ADQC was calculated using the following equation (Verma et al., 2014):

$$C_{dl} = (QR_{ct}^{1-n})^{1/n} \quad (5)$$

where Q is the constant phase element (CPE) ($\Omega^{-1}\, S^n\, cm^{-2}$), and n is the CPE exponent. Generally, the value of n is related to the surface heterogeneity or roughness. A low value of n is generally associated with high surface roughness. It is observed from the result depicted in Table 2 that the values of n are larger in the presence of ADQC (0.832–0.870) than in its absence (0.827), suggesting that surface roughness is remarkably improved owing to formation of protective film on metallic surface (Emran, 2014). Moreover, depending on the value of n, CPE can represent resistance ($n = 0$, $Y_0 = R$), capacitance ($n = 1$, $Y_0 = C$), inductance ($n = -1$, $Y_0 = 1/L$) or Warburg impedance ($n = 0.5$, $Y_0 = W$), where W is the Warburg parameter, the value of Warburg impedance (W_Z) related to the diffusion of the ions from the passive films of the inhibitor. Inspection of the Table 2 reveals that values of R_{ct} increase with increasing ADQC concentration suggesting that extent of surface coverage and η% increases with inhibitor concentration. The increased values of R_{ct} and decreased values of C_{dl} in the presence of ADQC are attributed either due to decrease in local dielectric constant or an increase in the thickness of electrical double layer or due to combined effect of both which is resulted due to adsorption of ADQC at metal/electrolyte interfaces.

Further, to get further information about adsorption of ADQC on metallic surface in 1 M HCl, Bode plots were

Table 2 EIS parameters obtained for mild steel in 1 M HCl in the absence and presence of different concentrations of ADQC.

Inhibitor	Conc (mg/L)	R_s (Ω cm^2)	R_{ct} (Ω cm^2)	C_{dl} (μF cm^{-2})	n	θ	η%
Blank	–	1.12	9.58	106.21	0.827	–	–
ADQC	5	0.81	40.91	103.57	0.832	0.4495	44.95
	10	0.902	101.39	53.03	0.846	0.9072	90.72
	15	0.732	159.3	46.38	0.853	0.9398	93.98
	20	0.904	206.59	39.81	0.863	0.9536	95.36
	25	1.364	247.53	36.83	0.870	0.9612	96.12

examined. Fig. 4b shows the Bode plots in the absence and presence of the ADQC. Bode plot gives a signal maxima (one time constant) at intermediate frequency region. Broadening of the signal maxima in the Bode plots is attributed due to adsorption of the ADQC on the metal/electrolyte interface (Zhao et al., 2015). In present study, the values of phase angle around −70° with slope values close to unity were obtained. Deviation from the ideal corrosive system (phase angle = 90° and slope = 1) is attributed due to surface roughness resulted due to structural and interfacial origin. However, in the presence of ADQC the values of phase angle increase with increasing concentration suggesting that the surface smoothness increases owing to the formation of the protective film by ADQC (Zhao et al., 2015).

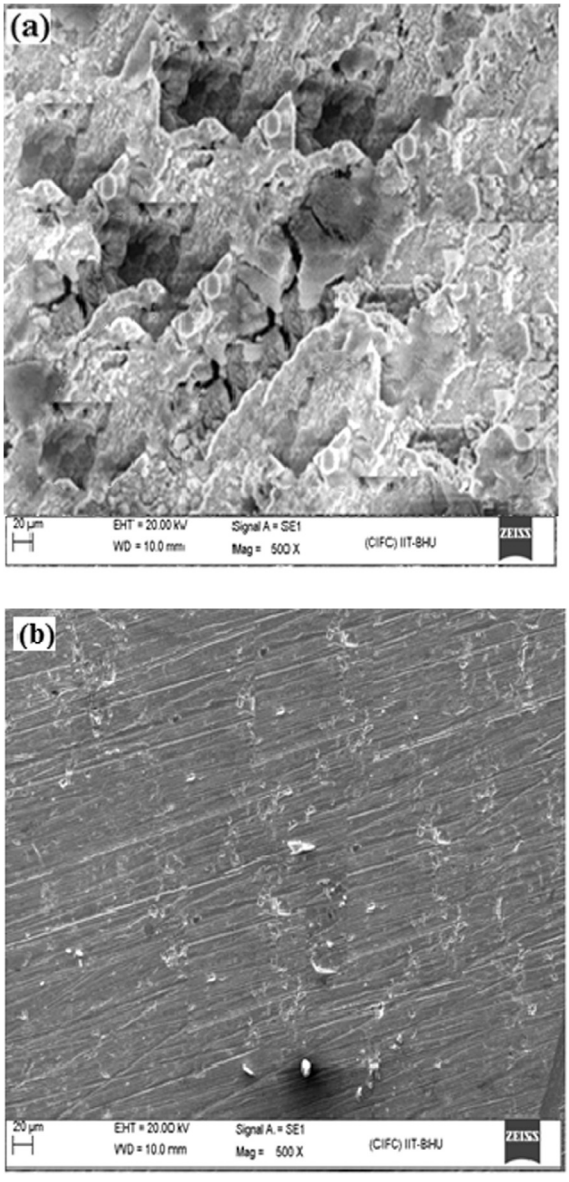

Figure 5 SEM micrographs of mild steel, (a) in the absence of ADQC and (b) in the presence of optimum concentration of ADQC.

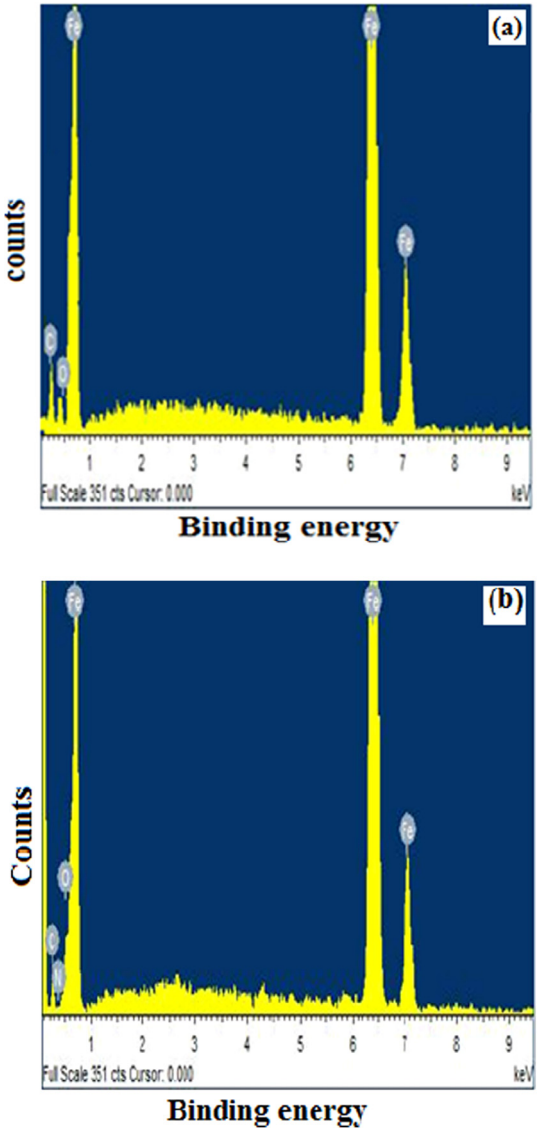

Figure 6 EDX spectra of mild steel, (a) in the absence of ADQC and (b) in the presence of optimum concentration of ADQC.

3.2. Surface measurements

3.2.1. Scanning electron microscopy (SEM) studies

The SEM micrographs of the SAE 1006 steel surface in the absence and presence of the ADQC at its optimum concentration after 3 h immersion time are shown in Fig. 5. Fig. 5a represents the SEM micrograph of the SAE 1006 steel surface in the absence of ADQC which is highly corroded and damaged. However, in the presence of ADQC (Fig. 5b) at optimum concentration, the surface morphology is remarkably improved due to adsorption of the ADQC on the mild steel surface which isolates the metal from the corrosive acid environment.

3.2.2. EDX studies

EDX spectra of SAE 1006 steel surface in the absence and presence of optimum concentration of ADQC are shown in Fig.6. Fig. 6a shows the EDX spectrum of the SAE 1006 steel surface in the absence of ADQC which showed characteristics signals only for Fe, C and O. The presence of low intensity signal for oxygen might be attributed due to formation of iron oxides during SEM-EDX operation. However, EDX spectrum of the surface in the presence of ADQC (Fig. 6b) shows additional signal for nitrogen. Moreover, the intensity for the signal corresponding to the oxygen further increased which suggested that ADQC adsorbed on the metal surface which resulted appearance of signals for N and O in EDX spectrum of inhibited SAE 1006 steel specimen.

3.2.3. Atomic force microscopy (AFM) studies

Fig. 7a represents the AFM micrograph of abraded SAE 1006 steel surface which is characterized by relatively smooth surface with abrading scratches on the surface. The calculated surface roughness of the abraded AFM micrograph was 85 nm. The AFM micrograph in the absence of ADQC (Fig. 7b) was highly corroded and damaged. The calculated surface roughness for uninhabited SAE 1006 steel specimen was 392 nm. However, in the presence of ADQC (Fig. 7c) the acid solution causes significant change in the surface smoothness of the AFM micrograph. From the AFM micrograph in the presence of ADQC it is concluded that it forms a surface film through adsorption which isolates the metal

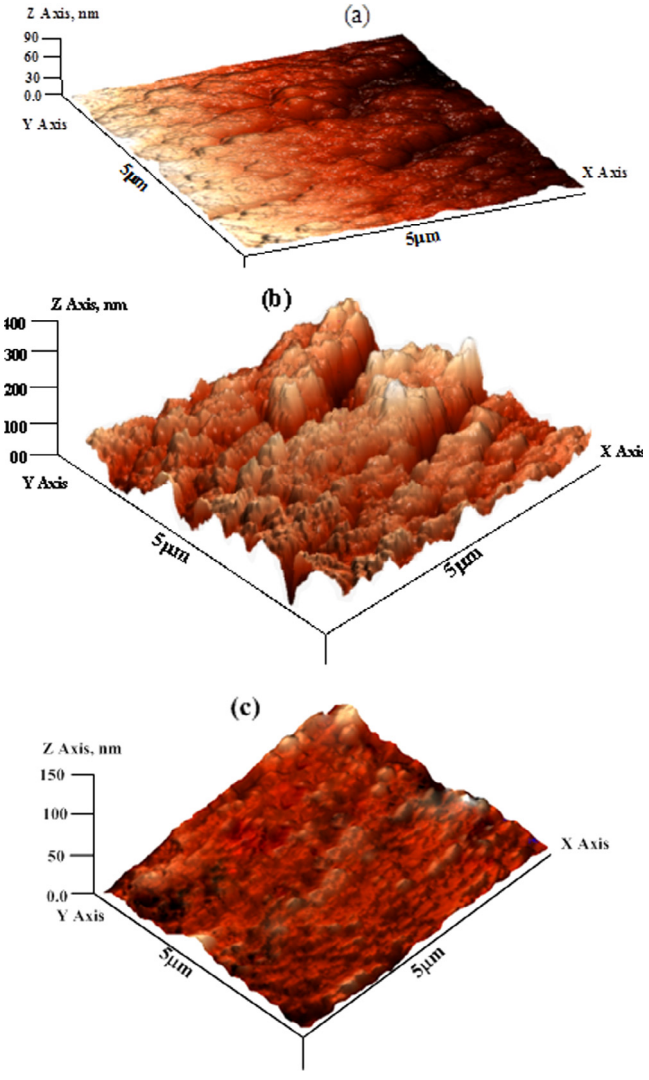

Figure 7 AFM micrographs of mild steel (a) abraded mild steel surface, (b) in the absence of ADQC and (c) in the presence of optimum concentration of ADQC.

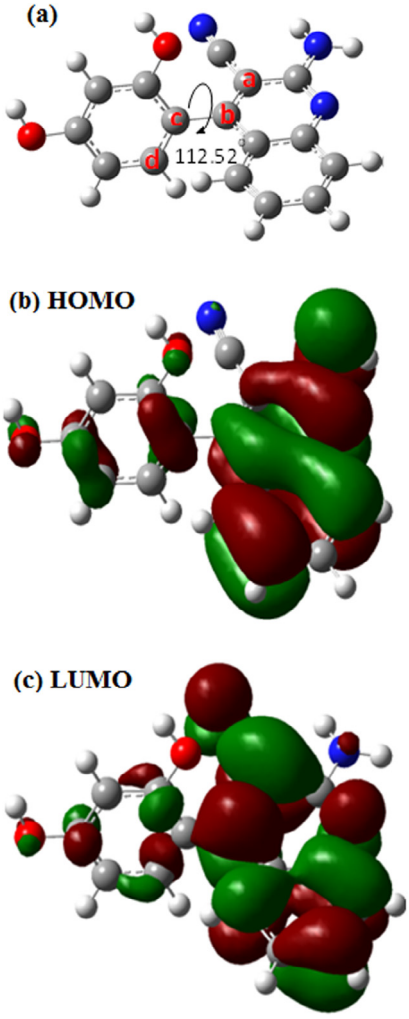

Figure 8 (a) Optimized structure of ADQC, (b) HOMO of ADQC and (c) LUMO of non-protonated ADQC.

Table 3 Quantum chemical parameters for investigated inhibitor (ADQC) in gas phase as well as in solution phase.

Parameters→ Compounds↓	E_{HOMO} (eV)	E_{LUMO} (eV)	ΔE (eV)	Hardness (σ)	Softness (ρ)	μ Debye
Non-protonated ADQC	−6.198	−2.233	3.964	1.982	0.5045	11.86
Protonated ADQC	−4.362	−1.362	3.000	1.500	0.666	8.126

from acid solution. The calculated surface roughness in the presence of ADQC was 137 nm.

3.3. Quantum chemical calculation

The values E_{HOMO}, E_{LUMO} and dipole moment (μ) were derived from geometrically optimized ADQC molecule (Fig. 8a). Fig. 8a and b represents the HOMO and LUMO frontier molecular orbital diagrams of the ADQC, respectively. From the calculated values of E_{HOMO} and E_{LUMO} the values of ΔE, global hardness (σ) and global softness (ρ) are calculated and given in Table 3. A very high value of E_{HOMO} (−6.198) and low value of E_{LUMO} (−2.233) suggest that ADQC has strong tendency to transfer its electrons to the appropriate empty d-orbitals of the surface atoms as well as to accept the electrons from the d-orbitals of the Fe-atoms in its pi-antibonding molecular orbitals (Banerjee et al., 2011). From the distribution of frontier molecular orbitals it can be seen that HOMO is mainly concentrated over the entire quinoline ring in addition to very slight distribution over dihydroxyphenyl ring. The involvement of the whole molecules in the electron transfer is attributed due to presence of the high electron density throughout the molecules in the form of non-bonding and π-electrons. However, it can be also observed that as compared to the dihydroxyphenyl ring, the quinoline ring is potentially more electrons donor as distribution of frontier molecular orbital mainly concentrated over quinoline ring. Thus, it concluded that the quinoline ring containing $-NH_2$ and –CN groups is comparatively softer part of the molecules and mainly involved in the electron transfer. Moreover, the LUMO distribution of frontier molecular orbitals indicated that similar to the electron transfer mainly by quinoline ring, the electrons acceptation is also mainly due to quinoline ring as distribution of frontier molecular orbitals of LUMO mainly concentrated over the quinoline ring. The energy band gap (ΔE) is another important parameter which can be used to correlate the structure of inhibitor with its inhibition efficiency. A small energy gap between the E_{LUMO} and E_{HOMO} suggests that the inhibitor has strong tendency to donate its electrons and exhibited high inhibition efficiency (Banerjee et al., 2011). Further, lower value of σ and high value of ρ also supported the strong interaction between metal and inhibitor. Moreover, the value of dipole moment (μ) is much higher (17.6170 Debye) as compared to the μ of water (1.85 Debye) suggesting that ADQC has much stronger tendency to adsorb on the SAE 1006 steel surface in aqueous acidic solution (Tang et al., 2009).

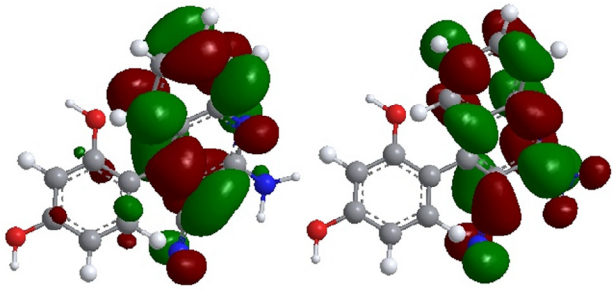

Figure 9 (a) Optimized structure of ADQC, (b) HOMO of ADQC and (c) LUMO of protonated ADQC.

The corrosion inhibition of metals by organic corrosion inhibitor was previously described by several authors. The ADQC easily protonates in acid solution due to presence of several N and O atoms. Fig. 9 represents the frontier molecular electron distribution of protonated ADQC. From the HOMO frontier molecular orbital electron distribution it can be seen that HOMO electron density mainly localized over quinoline ring. The 2,4-dihydroxyphenyl ring has very little contribution in HOMO. This finding suggests that quinoline moiety of the AQDC mainly contributes in the electron transfer. Moreover, from the LUMO frontier electron distribution, it can be seen the LUMO is also localized over the quinoline moiety; again the 2,4-dihydroxyphenyl ring has very little contribution in electron acceptation. The calculated quantum chemical parameters for protonated AQDC are given in Table 3. From the results depicted in the Table 3 it can be observed that parameters calculated for non-protonated and protonated AQDC are similar. The high value of E_{HOMO} and dipole moment and low value of E_{LUMO} are consistent with high inhibition efficiency of the AQDC. Similarly, the high value of global softness (ρ) and low value of global hardness (σ) suggest that the ADQC has strong tendency to adsorb on mild steel surface in 1 M HCl.

4. Conclusion

From the experimental and theoretical results it is concluded that investigated inhibitor acts as good corrosion inhibitor for SAE 1006 steel in 1 M HC. Its inhibition efficiency increases with increasing concentration and maximum efficiency was obtained at 25 mg/L concentration. EIS results suggested that ADQC forms surface film at metal/electrolyte interface. Tafel polarization study shows that ADQC acts as mixed type inhibitor. The SEM, EDX and AFM studies confirmed the formation of the surface protective film. The quantum chemical calculations well supported the experimental results and also show that ADQC has strong tendency to replace the water from metal surface.

References

Abd El-Lateef, H.M., 2015. Experimental and computational investigation on the corrosion inhibition characteristics of SAE 1006 steel by some novel synthesized imines in hydrochloric acid solutions. Corros. Sci. 92, 104–117.

Banerjee, S., Mishra, A., Singh, M.M., Maiti, B., Ray, B., Maiti, P., Maiti, B., Ray, B., Maiti, P., 2011. Highly efficient polyurethane ionomer corrosion inhibitor: the effect of chain structure. RSC Adv. 1, 199–205.

Beattie, C., North, M., Villuendas, P., 2011. Proline-catalysed amination reactions in cyclic carbonate solvents. Molecules 16, 3420–3432.

Becke, A.D., 1993. Density-functional thermochemistry. III. The role of exact exchange. J. Chem. Phys. 98, 5648–5652.

El Azzouzi, M., Aouniti, A., Herrag, L., Chetouani, A., Elmsellem, H., Hammouti, B., 2015. Investigation of isomers of hydroxyphenylamino propane nitrile as SAE 1006 steel corrosion inhibitors in 1 M HCl. Der. Pharma. Chem 7, 12–24.

Emran, K.M., 2014. Corrosion characterisation and passivation behavior of Fe68.6Ni28.2Mn3.2 alloy in acidic solution. Int. J. Electrochem. Sci. 9, 4217–4229.

Feng, L., Yang, H., Wang, F., 2011. Experimental and theoretical studies for corrosion inhibition of carbon steel by imidazoline derivative in 5% NaCl saturated Ca(OH)2 solution. Electrochim. Acta 58, 427–436.

Frisch, M.J., Trucks, G.W., Schlegel, H.B., Scuseria, G.E., Robb, M. A., Cheeseman, J.R., Scalmani, G., Barone, V., Mennucci, B., Petersson, G.A., et al, 2009. Gaussian 09, Revision D.01. Gaussian, Inc., Wallingford, CT.

Li, X., Deng, S., Fua, H., Li, T., 2009. Adsorption and inhibition effect of 6-benzylaminopurine on cold rolled steel in 1.0 M HCl. Electrochim. Acta 54, 4089–4098.

Martinez, S., 2003. Inhibitory mechanism of mimosa tannin using molecular modeling and substitutional adsorption isotherms. Mater. Chem. Phys. 77, 97–102.

Nezhad, A.K., Sarikhani, S., Shahidzadeh, E.S., Panahi, F., 2012. L-Proline-promoted three-component reaction of anilines, aldehydes and barbituric acids/malononitrile: regioselective synthesis of 5-arylpyrimido [4,5-b]quinoline-diones and 2-amino-4-arylquinoline-3-carbonitriles in water. Green Chem. 14, 2876–2884.

Olasunkanmi, L.O., Obot, I.B., Kabanda, M.M., Ebenso, E.E., 2015. Some quinoxalin-6-yl derivatives as corrosion inhibitors for SAE 1006 steel in hydrochloric acid: experimental and theoretical studies. J. Phys. Chem. C 119, 16004–16019.

Seikh, A.H., Sherif, E.M., 2015. Effects of immersion time and temperature on the corrosion of API 5L Grade X-65 Steel in 1.0 M H_2SO_4 pickling solution. Int. J. Electrochem. Sci. 10, 895–908.

Sheldon, R.A., 2005. Green solvents for sustainable organic synthesis: state of the art. Green Chem. 7, 267–278.

Sudheer, Quraishi, M.A., 2014. 2-Amino-3,5-dicarbonitrile-6-thio-pyridines: new and effective corrosion inhibitors for mild steel in 1 M HCl. Ind. Eng. Chem. Res. 53, 2851–2859.

Tang, Y.M., Yang, W.Z., Yin, X.S., Liu, Y., Wan, R., Wang, J.T., 2009. Phenyl-substituted amino thiadiazoles as corrosion inhibitors for copper in 0.5 M H_2SO_4. Mater. Chem. Phys. 116, 479–483.

Verma, C.B., Quraishi, M.A., Ebenso, E.E., 2013. Electrochemical studies of 2-amino-1, 9-dihydro-9-((2-hydroxyethoxy) methyl)-6H-purin-6-one as green corrosion inhibitor for SAE 1006 steel in 1.0 M hydrochloric acid solution. Int. J. Electrochem. Sci. 8, 7401–7413.

Verma, C.B., Reddy, M.J., Quraishi, M.A., 2014. Microwave assisted eco-friendly synthesis of chalcones using 2,4-dihydroxy acetophenone and aldehydes as corrosion inhibitors for SAE 1006 steel in 1 M HCl. Anal. Bioanal. Electrochem. 6, 321–340.

Verma, C.B., Singh, A., Pallikonda, G., Chakravarty, M., Quraishi, M.A., Bahadur, I., Ebenso, E.E., 2015a. Aryl sulfonamidomethylphosphonates as new class of green corrosion inhibitors for SAE 1006 steel in 1 M HCl: electrochemical, surface and quantum chemical investigation. J. Mol. Liq. 209, 306–319.

Verma, C.B., Quraishi, M.A., Singh, A., 2015b. 2-Aminobenzene-1,3-dicarbonitriles as green corrosion inhibitor for SAE 1006 steel in 1 M HCl: Electrochemical, thermodynamic, surface and quantum chemical investigation. J. Taiwan. Inst. Chem. Eng. 49, 229–239.

Verma, C.B., Singh, A., Quraishi, M.A., Singh, P., 2015c. A thermodynamical, electrochemical, theoretical and surface investigation of diheteroaryl thioethers as effective corrosion inhibitors for SAE 1006 steel in 1 M HCl. J. Taiwan. Inst. Chem. Eng. http://dx.doi.org/10.1016/j.jtice.2015.06.020.

Verma, C.B., Singh, P., Quraishi, M.A., 2016. A thermodynamical, electrochemical and surface investigation of Bis (indolyl) methanes as Green corrosion inhibitors for SAE 1006 steel in 1 M hydrochloric acid solution. J. Assoc. Arab. Univ. Basic Appl. Sci. 21, 24–30.

Yadav, D.K., Quraishi, M.A., 2012. Electrochemical investigation of substituted pyranopyrazoles adsorption on mild steel in acid solution. Ind. Eng. Chem. Res. 51, 8194–8210.

Yadav, M., Behera, D., Kumar, S., Sinha, R.R., 2013. Experimental and quantum chemical studies on the corrosion inhibition performance of benzimidazole derivatives for SAE 1006 steel in HCl. Ind. Eng. Chem. Res. 52, 6318–6328.

Zhao, J., Duan, H., Jiang, R., 2015. Synergistic corrosion inhibition effect of quinoline quaternary ammonium salt and Gemini surfactant in H_2S and CO_2 saturated brine solution. Corros. Sci. 91, 108–119.